



Prediction of critical heat flux for subcooled flow boiling

W. Liu^a, H. Nariyai^{b,*}, F. Inasaka^c

^a*Institute of Mechanical Engineering, Graduate School, University of Tsukuba, Tsukuba, Ibaraki 305-8573, Japan*

^b*Institute of Engineering Mechanics and Systems, University of Tsukuba, Tsukuba, Ibaraki 305-8573, Japan*

^c*Nuclear Technology Division, Ship Research Institute, Mitaka, Tokyo 181-0004, Japan*

Received 28 May 1999; received in revised form 15 November 1999

Abstract

A theoretical critical heat flux (CHF) prediction model is developed for the subcooled flow boiling based on the liquid sublayer dryout mechanism. The model is tested over a large data bank (about 2482 points), which is characterized by covering almost the entire physics scope, showing a general good accuracy. Parametric trends of the CHF in terms of mass flux, pressure, subcooling, channel diameter and ratio of heated length to diameter are studied with the aim of not only indicating the trends, but also giving the theoretical interpret. The model also shows good adaptation to non-uniform heating, twist tape insert and non-water (nitrogen and refrigerant 113) system. © 2000 Elsevier Science Ltd. All rights reserved.

Keywords: Subcooled flow boiling; Critical heat flux; Mechanism model; Parametric study

1. Introduction

The ability to predict critical heat flux (CHF) well is of considerable interest to nuclear reactor technology. Although the modelling of the CHF for subcooled flow boiling can be categorized into six groups, as pointed in Ref. [1], currently only bubble crowding mechanism [2–4] and liquid sublayer dryout mechanism [5–7] are receiving significant attention.

Liquid sublayer dryout mechanism assumes that, a vapor blanket, which is formed as a consequence of coalescence of small bubbles rising along the near wall region, is overlying a very thin liquid sublayer adjacent to the wall (Fig. 1). The CHF is assumed to happen at the complete dryout of liquid sublayer. As the result, CHF is described as:

$$\text{CHF} = \frac{\rho_l \delta H_{fg}}{L_B} U_B \quad (1)$$

where U_B , L_B , and δ are the vapor blanket velocity, vapor blanket length and thickness of liquid sublayer, respectively. The vapor blanket length is assumed to be equal to the Helmholtz critical wavelength, which is inversely proportional to U_B^2 as:

$$L_B \propto \frac{1}{U_B^2} \quad (2)$$

Then CHF is written in:

$$\text{CHF} = KU_B^3 \delta \quad (3)$$

So, the key for the liquid sublayer dryout mechanism turns to the calculation of U_B and to the calculation of δ . Different models employed different ways.

Lee and Mudawar [5] calculated δ by a force balance on the vapor blanket in radial direction. Three

* Corresponding author.

Nomenclature

A	defined in Eqs. (10f) and (10h) (dimensionless)	Z_0	the length from tube inlet to NVG point (m)
C_D	drag coefficient (dimensionless)	Z_{sb}	significant boiling length, calculated by $(L - Z_0)$
C_p	specific heat at constant pressure (J/kg K)		
CHF	critical heat flux (W/m ²)		
D	tube inner diameter (m)	<i>Greek symbols</i>	
f	friction factor (dimensionless)	α	void fraction (dimensionless)
g	gravitational acceleration (m/s ²)	δ	initial liquid sublayer thickness (m)
G	mass flux (kg/m ² s)	ε	surface roughness (m)
H	enthalpy (J/kg)	η	wave height (m)
H_{fg}	latent heat of vaporization (J/kg)	ϕ	velocity potential
h_1	Dittus–Boelter’s liquid heat transfer coefficient	λ	wavelength (m)
h_{1-A}	subcooled liquid-phase heat transfer coefficient in Ahmad model	ρ	density (kg/m ³)
K	proportional constant in Eq. (3)	γ	twist ratio of tape
k_1	liquid thermal conductivity (W/mk)	σ	surface tension (N/m)
L	length (m)	τ	passage time of vapor blanket (s)
NVG	net vapor generation	τ_w	wall shear stress (MPa)
P	system pressure (MPa)	μ	viscosity (kg/ms)
Pr	Prandtl number (dimensionless)	χ	true quality (dimensionless)
Re	Reynolds number	χ_d	thermal equilibrium quality at NVG point
q	heat flux (W/m ²)	χ_{eqout}	thermal equilibrium quality at exit point
S	slip ratio (dimensionless)		
T	temperature (K)	<i>Subscripts</i>	
U	velocity (m/s)	1	at interface I
U_τ	friction velocity (m/s)	2	at interface II
U^+	non-dimensional velocity	avg	average
ΔT	liquid subcooling (K)	B	vapor blanket
V_c	bulk average velocity (m/s)	c	core region
V_1	liquid velocity in straight tube (m/s)	d	net vapor generation point
V_{y1}	resultant velocity by Gambill in Eq. (19)	eq	thermal equilibrium
y	distance from the heated wall to the bubble central line (m)	f	liquid at saturation
y^+	non-dimensional distance from heated wall	g	gas
y^*	superheated layer thickness in Celata model (m)	in	tube inlet
		l	liquid
		out	tube exit
		max	maximum
		min	minimum

empirical constants are used in the process. The model was found to be unable to give accurate CHF predictions at low pressure.

Katto [6] calculated U_B by using empirical based relation (as a function of Reynolds number, liquid and vapor density and void fraction) and evaluated δ using a correlation for pool boiling [8]. The Katto model is not able to calculate the CHF in those cases where the local void fraction in the near-wall bubbly layer is higher than 70% [1].

Celata et al. [7] assumed the vapor blanket developed and existed only in the near-wall region where the local liquid temperature is higher than satur-

ation temperature. δ is calculated by subtracting the vapor blanket diameter D_B from the superheated liquid thickness y^* . The model is successful in predicting the CHF at low-medium pressure. For the first time, no empirical constant, which is created to coincide the CHF experimental data, is employed in the calculation process. However, the model shows a little deficiency in the CHF prediction at low L/D condition [9] or at high-pressure condition.

Recently, Celata [10] raised a superheated layer vapor replenishment model. The new model approaches CHF almost the same procedure and therefore results in almost same CHF prediction as the

old one. It still cannot overcome the defect mentioned above.

In view of the above-described limitations of the Lee–Mudawar, Katto and Celata models, a new model is developed with the aim of accuracy, simplicity and clear physics meaning.

2. The proposed model

Let us first give a brief depiction to the formation of a stable vapor blanket. As we know, bubbles detach tube wall frequently in the onward region of net vapor generation (NVG) point. Vapor blankets are formed as the consequence of coalescence of the small bubbles. As assumed by Lee and Mudawar [5], the development of each blanket is strongly limited by neighboring blankets that tend to confine the blanket circumferential growth. It is, therefore, reasonable to assume the diameter of the vapor blanket is approximately equal to the diameter of the bubble at the departure from the wall. The departing bubbles are assumed to coalesce into a long blanket, which maintains a fairly constant equivalent diameter while stretching in the direction of fluid flow due to the generation of more vapors by sublayer evaporation.

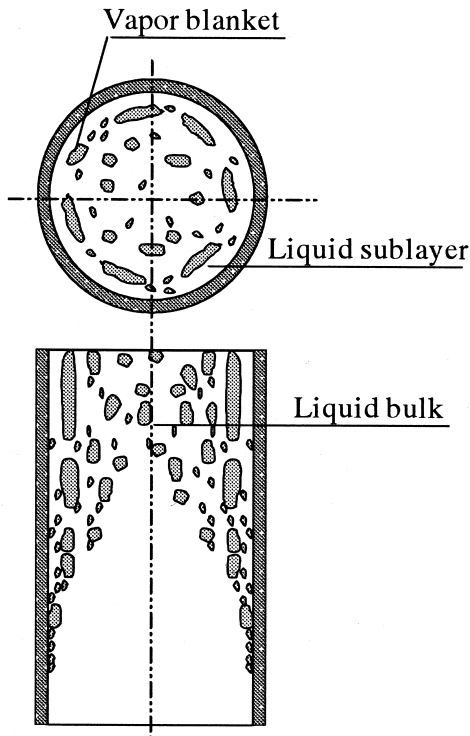


Fig. 1. Conceptual view of liquid sublayer dryout mechanism.

Considering waves existing both at interfaces I (the interface of the liquid sublayer and the vapor blanket) and II (the interface of the vapor blanket and the core region), as shown in Fig. 2, we assume that the two waves are always of same wavelength (see Appendix B for the mathematical demonstration). The two wavelengths are assumed to be equal to the Helmholtz instability wavelengths at interfaces I and II, respectively. A stable vapor blanket is assumed containing only one complete wavelength (otherwise, as analyzed in the last part of the Appendix B, if a vapor blanket contains more than one wavelength, the blanket would be unstable and has the tendency to break down to form the stable vapor blanket at its thinnest points when the two waves come to opposite phases). With these assumptions, the vapor blanket length L_B can be written as $L_B = \lambda_1 = \lambda_2$.

The vapor blanket divides flow area into two parts (Fig. 2). One is near wall region filled with superheated liquid and is called liquid sublayer. The other is core region that is filled with gas–liquid two-phase flow. The CHF is assumed to happen when the meniscus liquid sublayer is extinguished by evaporation during the passage time of the vapor blanket $\tau = L_B/U_B$.

From the above-mentioned assumptions, by writing the Helmholtz critical wavelengths to both the interfaces and by supposing they are equal to each other, the vapor blanket velocity can be written as a simple function of the core region two-phase flow average velocity that can be got by the knowledge we have

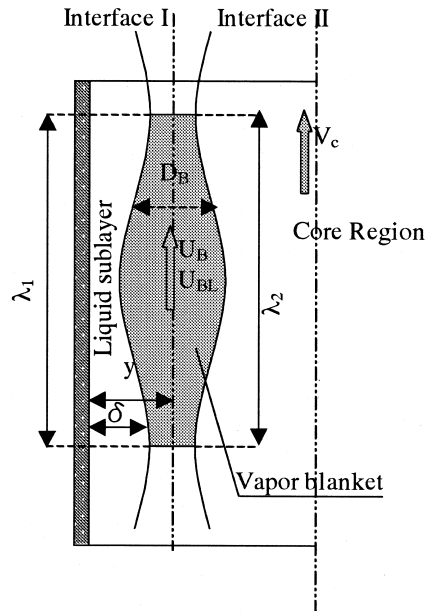


Fig. 2. Schematic representation of a stable vapor blanket in the proposed model.

known. The vapor blanket length is then calculated simply from the expression of the Helmholtz instability wavelength. The sublayer thickness is obtained from Karman velocity distribution equations if the liquid velocity at the centerline of the vapor blanket, U_{BL} , is known. U_{BL} is calculated as the difference of the vapor blanket velocity, U_B , and the relative vapor blanket velocity determined by the balance between buoyancy and drag forces exerted on the vapor blanket [5].

The above thought, based only on a fundamental physical consideration, is the main difference between the current model and those proposed by predecessors.

2.1. Vapor blanket velocity U_B

First write the critical Helmholtz instability wavelength at the interface I. Because the liquid sublayer is near the tube wall and always be very thin, the average velocity in the liquid sublayer is assumed to be 0. The critical Helmholtz wavelength at interface I, therefore, can be written as:

$$\lambda_1 = \frac{2\pi\sigma}{\rho_g U_B^2} \quad (4)$$

Second, write the Helmholtz critical wavelength at the interface II as:

$$\lambda_2 = \frac{2\pi\sigma(\rho_c + \rho_g)}{\rho_c \rho_g (V_c - U_B)^2} \quad (5)$$

Considering the assumption that the two waves are of the same wavelength, we get $\lambda_1 = \lambda_2$. Then U_B is got as:

$$U_B = \frac{V_c}{1+b} \quad (6)$$

where

$$b = \sqrt{(\rho_c + \rho_g)/\rho_c} \quad (6a)$$

If the CHF is assumed to occur at the tube exit, V_c and ρ_c are the core region two-phase average velocity and average density at the tube exit, respectively. V_c can be simply calculated from:

$$V_c = G/\rho_c \quad (7)$$

ρ_c is calculated from:

$$\rho_c = (1 - \alpha_c)\rho_{lout} + \alpha_c \times \rho_g \quad (7a)$$

Where α_c and ρ_{lout} are the exit core region void fraction and liquid density, respectively. From the calculation results, the liquid sublayer thickness and vapor blanket diameter are always shown to be very thin, α_c

therefore can be written simply as:

$$\alpha_c = \alpha_{out} \quad (7b)$$

The evaluation of α_{out} can be obtained either by Ahmad [11] or Kroger–Zuber [12] or Dix [56] models. Present authors tested all the models and found no very big difference exists in the prediction results. With the Ahmad model, α_{out} is given as:

$$\alpha_{out} = \frac{\chi_{out}}{\chi_{out} + \left(\frac{\rho_g}{\rho_f}\right)S(1 - \chi_{out})} \quad (8)$$

where S is slip ratio and is expressed as:

$$S = \left(\frac{\rho_f}{\rho_g}\right)^{0.205} \left(\frac{GD}{\mu_f}\right)^{-0.016} \quad (8a)$$

χ_{out} is exit true quality and can be calculated either from Jafri et al. [39] model (Eq. (9)) or the model recommended by Ahmad [11], Saha and Zuber [14] or Levy [13] (Eq. (10)). Although the latter one is thought to be only an approximation of the former, the latter is adopted because it has been well accepted.

$$\frac{dx}{dx_{eqout}} = 1 + \frac{x - x_{eqout}}{(1-x)x_d} \quad (9)$$

with initial condition:

$$\text{at NVG point } (\chi_{eqout} = \chi_d), \quad \chi = 0 \quad (9a)$$

$$\chi_{out} = \frac{\chi_{eqout} - \chi_d \exp\left(\frac{\chi_{eqout}}{\chi_d} - 1\right)}{1 - \chi_d \exp\left(\frac{\chi_{eqout}}{\chi_d} - 1\right)} \quad (10)$$

where χ_{eqout} and χ_d are the thermal equilibrium quality at the tube exit and the NVG point, respectively.

$$\chi_{eqout} = \left(H_{lin} + \frac{4qL}{GD} - H_f\right)/H_{fg} \quad (10a)$$

It seems χ_{eqout} is the function of pressure P , mass velocity G , inlet liquid thermal condition and the ratio of the heated length to the inside diameter L/D . If L/D is maintained as a certain value, χ_{eqout} shows no relation with D .

χ_d is calculated from:

$$\chi_d = (H_{ld} - H_f)/H_{fg} = -C_{pl, T_d} \Delta T_d / H_{fg} \quad (10b)$$

The NVG point is normally given in terms of a critical subcooling as ΔT_d . Ahmad [11], Levy [13] and Saha and Zuber [14] raised different models for the NVG point prediction. It seems the NVG is basically a function of P , D , G and showed no relation with the

heated length L . It is found that in the proposed model, either the Levy model or the Ahmad model can be used. With the Ahmad model, the NVG is calculated from:

$$\Delta T_d = q/h_{1-A} \tag{10c}$$

where h_{1-A} is calculated by:

$$h_{1-A} = 2.44 \frac{k_f}{D} \left(\frac{GD}{\mu_f} \right)^{1/2} \left(\frac{C_{pl, T_d} \mu_f}{k_f} \right)^{1/3} \left(\frac{H_{lin}}{H_f} \right)^{1/3} \left(\frac{H_{fg}}{H_f} \right)^{1/3} \tag{10d}$$

If the calculated ΔT_d is higher than the inlet subcooling ($\Delta T_d > \Delta T_{in}$), which means the physically valid NVG point is tube inlet, ΔT_d is substituted by the value of ΔT_{in} .

As to the exit liquid temperature T_{out} , Ahmad [11], Staub [15] and Kroger and Zuber [12] recommended almost the same exponential expression as:

$$\Delta T_{out} = \Delta T_d e^{-A} \tag{10e}$$

where A has a special physical meaning as the ratio of the heat absorbed by the liquid from the NVG point to the tube exit to the whole heat needed to raise the liquid at the NVG to saturation. In the Ahmad model, A is written as:

$$A = \frac{q^* Z_{sb}}{GDC_{pl, T_d} \Delta T_d / 4} \tag{10f}$$

where Z_{sb} is significant boiling length and is calculated as the difference of heated length L and Z_0 , the length from the tube inlet to the NVG point, as:

$$Z_{sb} = L - Z_0$$

$$Z_0 = GDC_{pl, T_d} \frac{\Delta T_{in} - \Delta T_d}{4q} \tag{10g}$$

With rearrangement, A also can be written as:

$$A = 4q \left[\frac{L}{D} - \frac{G(H_{ld} - H_{lin})}{4q} \right] / [G(H_f - H_{ld})] \tag{10h}$$

2.2. Liquid sublayer thickness

2.2.1. Calculation of L_B and D_B

With U_B calculated, L_B is calculated from:

$$L_B = \lambda_1 = \lambda_2 = \frac{2\pi\sigma}{\rho_g U_B^2} \tag{11}$$

The diameter of vapor blanket is calculated from the Levy model [13] as:

$$D_B = 0.015 \left(\frac{\sigma D}{\tau_w} \right)^{0.5} \tag{12}$$

where

$$\tau_w = \frac{fG^2}{8\rho_f} \tag{12a}$$

The friction factor f , calculated by Colebrook equation [16], is written as:

$$\frac{1}{\sqrt{f}} = 1.14 - 2.0 \log \left(\frac{\varepsilon}{D} + \frac{9.35}{Re\sqrt{f}} \right) \tag{13}$$

where ε is the surface roughness, which is assumed to be close to $0.75D_B$ in Celata model [7]. Considering $\varepsilon = 0.75D_B$, making use of Eq. (12), Eq. (13) then turns to:

$$\frac{1}{\sqrt{f}} = 1.14 - 2.0 \log \left(0.75 \times 0.015 \sqrt{\frac{8\sigma\rho_f}{fG^2 D}} + \frac{9.35}{Re\sqrt{f}} \right) \tag{13a}$$

2.2.2. Calculation of U_{BL}

As reported by Lee and Mudawar [5], the velocity of the vapor blanket in vertical turbulent flow can be obtained by a force balance, i.e. buoyancy and drag forces as:

$$\frac{\pi}{4} D_B^2 L_B g (\rho_f - \rho_g) = \frac{1}{2} \rho_f C_D (U_B - U_{BL})^2 \frac{\pi D_B^2}{4} \tag{14}$$

With rearrangement:

$$U_{BL} = U_B - \left(\frac{2L_B g (\rho_f - \rho_g)}{\rho_f C_D} \right)^{0.5} \tag{15}$$

Drag coefficient C_D can be obtained either by Harmathy [17] or Chan and Prince [18] expressions. The former determined by buoyancy and surface tension forces is recommended in the present model at low pressure ($P < 1$ MPa). The latter one proposed for small bubble that is dominated by viscous forces is recommended at medium and high pressure ($P \geq 1$ MPa).

$$\text{Harmathy: } C_D = \frac{2}{3} \frac{D_B}{\left(\frac{\sigma}{g(\rho_f - \rho_g)} \right)^{0.5}} \tag{15a}$$

$$\text{Chan and Prince: } C_D = \frac{48\mu_f}{\rho_f D_B (U_B - U_{BL})} \tag{15b}$$

Table 1
Data collected by Celata

Reference	No. of data	G (Mg/m ² s)	P (MPa)	D (mm)	L/D	T_{in} (°C)	q_{exp} (MW/m ²)
Celata et al. [19]	268	2.0–40.0	0.1–5.0	2.5–8.0	12.5–40.0	18.6–81.0	4.0–60.6
Inasaka-Nariai [41]	29	4.3–30.0	0.3–1.1	3	33.3	25.0–78.0	7.3–44.5
Nariai et al. [31]	95	6.7–20.9	0.1	1.0–3.0	3–50	15.4–64.0	4.6–70.0
Boyd [42,28,43]	10	4.4–40.5	0.77–1.66	3	96.57	20.0	6.0–41.5
Achillib [44]	35	4.6–14.9	1.0–5.5	8.0–15.0	15–20	26.4–158.0	11.0–35.6
Gambill [45]	7	13.0–26.0	0.1	7.8	9–20	4.9–35.8	15.8–33.0
Vanderfort [29]	210	8.4–42.7	0.1–2.3	0.3–2.6	2.5–26.0	6.4–85.0	18.7–123.8
Loosmore [46]	202	3.0–2.0	0.1–0.7	0.6–2.4	3–50	3.2–131.0	6.7–44.8
Ornatskii [40]	125	10.0–90.0	1.1–3.2	0.4–2.0	28	6.7–156.0	27.9–227.9
Ornatskii [47]	117	5.0–30.0	1.0–2.5	2	28	2.7–205.0	6.4–66.6
Ornatskii [48]	68	20.0–90.0	1.0–3.2	0.5	28	1.5–154.0	41.9–224.5
Knoebel et al. [37]	376	3.9–13.7	0.2–0.7	9.5	64	0.3–105.0	3.3–11.4
Mirshak et al. [49]	56	4.7–12.2	0.2–0.6	6.0–11.9	41–96	4.7–12.0	3.9–10.0
Babcock [50]	57	2.4–11.4	0.4–8.4	7.9–25.4	27–75	19.9–243.0	4.9–11.8
Burck [51]	143	0.9–3.8	1.1–3.1	10	35	16.7–601.0	4.5–12.2
Mayersak [52]	1	44.4	2.9	11.7	50	18.0	42.8
Schaefer [53]	2	61.2–62.0	1.3–1.5	3.05	6.25	15.6–19.0	125.0–130.0
Thorgerson [54]	42	4.2–13.4	0.5	7.8–8.4	72–78	1.1–79.0	4.2–12.4
Zergarnik [55]	21	4.8–20.6	0.5–3.0	4	62.5	0.6–134.0	9.4–32.6
Gambill [33]	23	7.0–53.0	0.1–0.5	3.2–7.8	6–54	8.8–24.0	7.0–48.7
Total	1887	0.9–90.0	0.1–8.4	0.3–25.4	2.5–97.0	0.3–243.0	3.3–227.9

2.2.3. Calculation of liquid sublayer thickness δ

By knowing U_{BL} , the distance y , which is the distance from wall to the bubble centerline (Fig. 2), can be got from the Karman velocity distribution equation as:

$$\begin{cases} U_{BL}^+ = y^+ & 0 \leq y^+ < 5 \\ U_{BL}^+ = 5.0 \ln y^+ - 3.05 & 5 \leq y^+ < 30 \\ U_{BL}^+ = 2.5 \ln y^+ + 5.5 & y^+ \geq 30 \end{cases} \quad (16)$$

where $U_{BL}^+ = \frac{U_{BL}}{U_\tau}$, $U_\tau = (\frac{\tau_w}{\rho_f})^{0.5}$, $y^+ = y \frac{U_\tau}{\mu_f} \rho_f$, $\tau_w = \frac{fG^2}{8\rho_f}$

Then δ is got from

$$\delta = y - D_B/2 \quad (17)$$

2.3. Calculation of CHF

The critical heat flux is calculated from:

$$CHF = \frac{\rho_f \delta H_{fg}}{L_B} U_B \quad (18)$$

For a given geometric and inlet thermal hydraulic condition, the critical heat flux can be predicted by an iterative procedure through the forgoing equations (see Appendix A for detailed information).

3. Verification of the CHF model

To verify the proposed model, a very big database is collected (Tables 1–4). The data come from three sources. The first one is Celata database [19] (Table 1) with totally 1887 data points. The second is Pei database [30] (Table 2) with totally 486 data points. The third is the data proposed by Chen et al. [27] (Table 3) recently with 109 data points.

Fig. 3 shows a comparison of calculated versus experimental CHF, using the above databases. About 89% of data are predicted within $\pm 30\%$. The verifica-

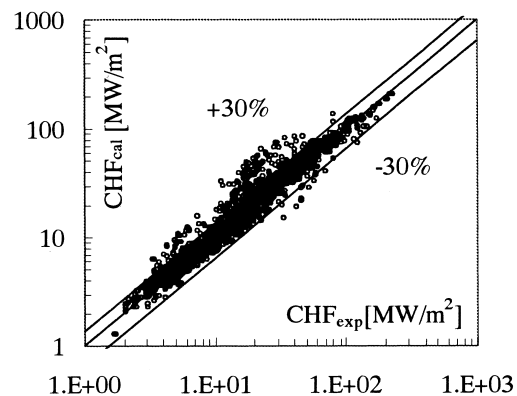


Fig. 3. Calculated vs. experimental CHF.

Table 2
Data collected by Pei

Reference	No. of data	G (Mg/m ² s)	P (MPa)	D (mm)	L/D	T_{in} (°C)	q_{exp} (MW/m ²)
Bortoli [20]	153	1.2–10.6	3.5–19.25	1.9–5.7	20–365	27–354	1.7–13.3
Matzner [21]	76	1.36–18.6	7	12.8–37.5	25.8–151.0	116–270	3.1–8.1
Lee [22]	23	2.0–4.1	3.9–11.3	5.6–10.8	20–82	181–254	3.9–7.2
Thompson [23]	146	3.7–10.4	3.5–10.5	10.3	74.26–77.0	202–251	4.19–9.4
Weatherhead [24]	9	6.5–9.3	2.17	1.1	100	102–173	4.26–7.3
Weatherhead [25]	76	0.9–2.7	14	7.7–11.1	41.3–59.2	67–302	2.52–5.3
Hood [26]	3	1.7–2.4	7	12.4–23.5	26–49	162–252	3.4–4.9
Total	486	0.9–18.6	2.17–19.25	1.1–37.5	20–365	27–354	1.7–13.3

tion shows the proposed model is valid through a wide range of operating condition.

With reference to the model raised by Celata [7], comparisons between the Celata model and the present model are accomplished. The percentages of data points calculated with a given error band (%) are plotted, against the error band, using the Celata database only, the Pei database only and all the databases. Although the proposed model shows a little worse prediction than the Celata model with the Celata database in Fig. 4(a), it shows a much better prediction with the Pei database (Fig. 4(b)) and a general better prediction than the Celata model is obtained with all the databases (Fig. 4(c)).

Fig. 5(a)–(f) show the ratio of the calculated to the experimental CHF versus the mass flux, pressure, inlet subcooling, exit equilibrium quality, diameter and L/D , to ascertain possible systematic effects in the model behavior. No systematic error of CHF prediction versus G , P , ΔT_{in} , x_{eqout} and D are observed. But an over prediction of the CHF is observed at low L/D ($L/D < 20$, Fig. 5(f)), especially at the high system pressure condition. The possible reasons are analyzed as: (1) The error in the calculations of the NVG point, exit true quality and void fraction. As we know, all the correlations for the calculation of the NVG point, true quality and void fraction are something empirical and were developed for the thermal hydraulic fully developed region. So, their suitability at low L/D condition, where thermal hydraulic is far from fully developed, is quite doubtful. (2) The change of the triggering mechanism for the CHF occurrence. The low L/D condition always results in extremely high CHF, which is found may be triggered by some other mechanism.

Table 3
Chen data

Reference	No. of data	G (Mg/m ² s)	P (MPa)	D (mm)	L/D	T_{in} (°C)	q_{exp} (MW/m ²)
Chen et al. [27]	109	1.4–13.0	0.16–1.29	10–16	18.4–40.0	19–114	4.17–10.4

The model shows significant ability for the non-low L/D -data prediction. With still above three databases (totally 2482 points), with omitting low L/D data ($L/D < 20$, totally 283 points), about 34% of data points are predicted within $\pm 5\%$, 58% are predicted within $\pm 10\%$ and about 96% are predicted within $\pm 35\%$.

It has to be specified that, with different model adoptions for the NVG point, true quality and void fraction calculations, the proposed model give different prediction result. All the listed results are got with the model adoption same as what shown in the Appendix A. And with the changing of model adoption for the NVG point, true quality and void fraction, the proposed model may give even better prediction (for example, with replacing the Ahmad model for the true quality with Jafri model [39]; or at low L/D condition, with replacing the Ahmad model for the void fraction with the Dix model [56]).

4. Comparison of the present model with the Celata model

Far by now, the Celata model [7] can be said the best model. In the following, the comparisons for the predictions of the CHF and some important parameters between the two models are carried out.

4.1. Comparison of CHF data

Fig. 6(a) and (d) show the comparisons of the CHF predictions by the present and the Celata models.

Table 4
Total data used for the model verification

	No. of data	G (Mg/m ² s)	P (MPa)	D (mm)	L/D	T_{in} (°C)	q_{exp} (MW/m ²)
Total	2482	0.9–90.0	0.1–19.25	0.3–37.5	2.5–365	0.3–354.0	3.3–227.9

From the figures, we can see that at low pressure, the two models give almost the same CHF predictions although the basic thought of the two models differs

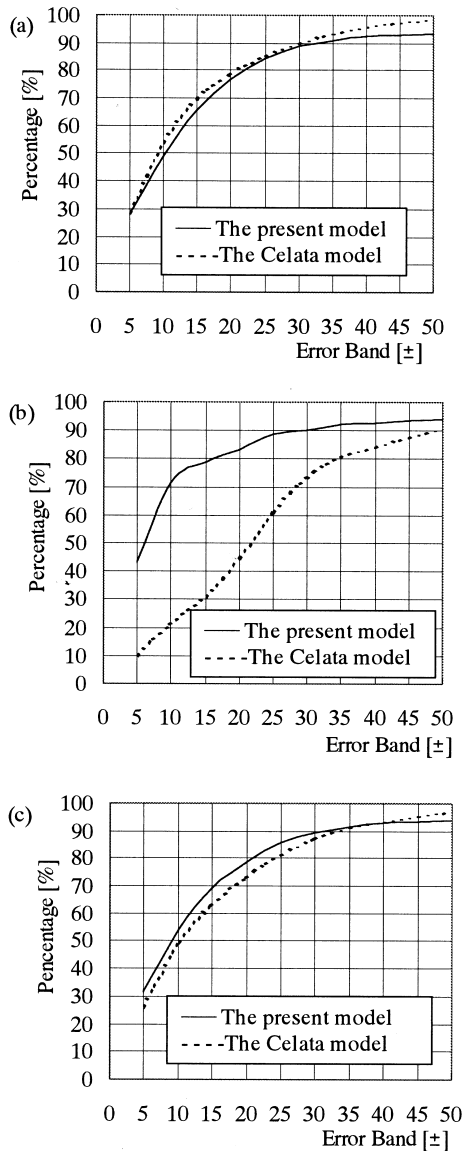


Fig. 4. Comparisons of the CHF prediction ability between the present model and the Celata model (a) with only the Celata database; (b) with only the Pei database; (c) with all the databases.

greatly. At high pressure, the Celata model has a little tendency to give low predictions.

4.2. Comparisons of U_B (Fig. 6(b) and (e)) and δ (Fig. 6(c) and (f))

The calculation of U_B and δ is the main difference between the two models. The present model considers gas and liquid phases separately. With the assumption that the same wavelengths at the two liquid–gas interfaces, U_B is calculated first. δ is calculated on the base of U_B . Celata gave the δ as the difference of the superheated layer thickness and the vapor blanket diameter. In the Celata model, U_B is obtained on the base of δ . It is interesting to see that U_B and δ are obtained with no big difference even though the calculation process differs greatly.

4.3. Comparison of D_B and L_B (Fig. 6(c) and (f))

In the D_B calculation, Celata adopted the Staub model, in which D_B is inversely proportional to G^2 . The present model adopts the Levy model, in which D_B is inversely proportional to G . As to the L_B calculation, two models both employed the Helmholtz instability wavelength that is inversely proportional to U_B^2 .

5. Parametric trends of the CHF

As we have known, CHF is a function of thermal hydraulic conditions (G , P and ΔT_{in}) and geometric parameters (D and L/D). This paper intends to study parametric trends from the model theory viewpoint, with the aim of not only indicating the parametric trends, but also giving the reason for the trends. Experimental data are also plotted for comparison if corresponding data are available.

5.1. The thermal hydraulic conditions (G , P and ΔT_{in})

G , P and ΔT_{in} effects on the CHF have been investigated a lot. It is well known that CHF is an increasing function of G and ΔT_{in} , and has little relationship with P in the subcooled flow boiling. In the proposed model, G and P are employed in almost every step of the CHF prediction and affect CHF from comprehen-

sive ways. The increase of inlet subcooling ΔT_{in} directly ameliorates exit bulk thermal condition (decrease χ_{out} , α_{out} and T_{out}) and so makes tube be able to endure a higher heat flux. Fig. 7(a)–(c) show the calculated CHF versus G , P and ΔT_{in} , respectively with the comparison to experimental data. The model shows providing the same observed experimental

trends of CHF versus mass velocity, pressure and inlet subcooling.

5.2. The geometric parameters (D and L/D)

Paying a little attention to the model calculation procedures, we can find that the every appearance of

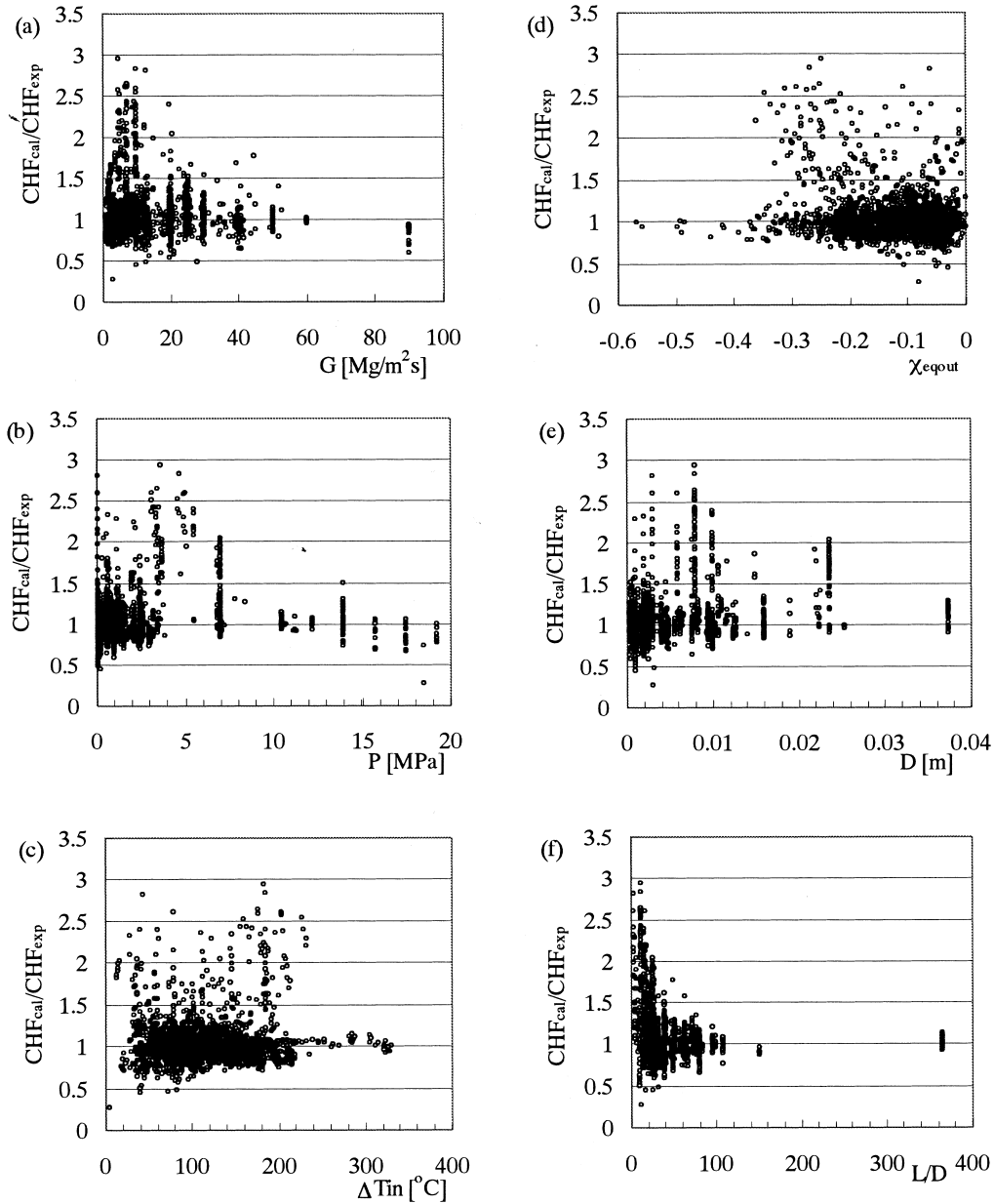


Fig. 5. Ratio of the calculated to experimental CHF vs.: (a) mass flux; (b) pressure; (c) inlet subcooling; (d) exit equilibrium quality; (e) inner diameter; (f) ratio of the heated length to the diameter L/D .

the heated length L is accompanied by the appearance of the inner diameter D (Eqs. (10a) and (10h)). They work together to affect CHF prediction with the form of L/D . So, it's reasonable to use L/D as a characteristic parameter. This makes that in the discussion of D effect on CHF, it's L/D , not L , should be kept at a

certain value. Otherwise the showing effect would be the effects of both D and L/D . The same should be paid attention in the discussion of the L/D effect.

5.2.1. Inner diameter D

The D effect on the CHF had been discussed a

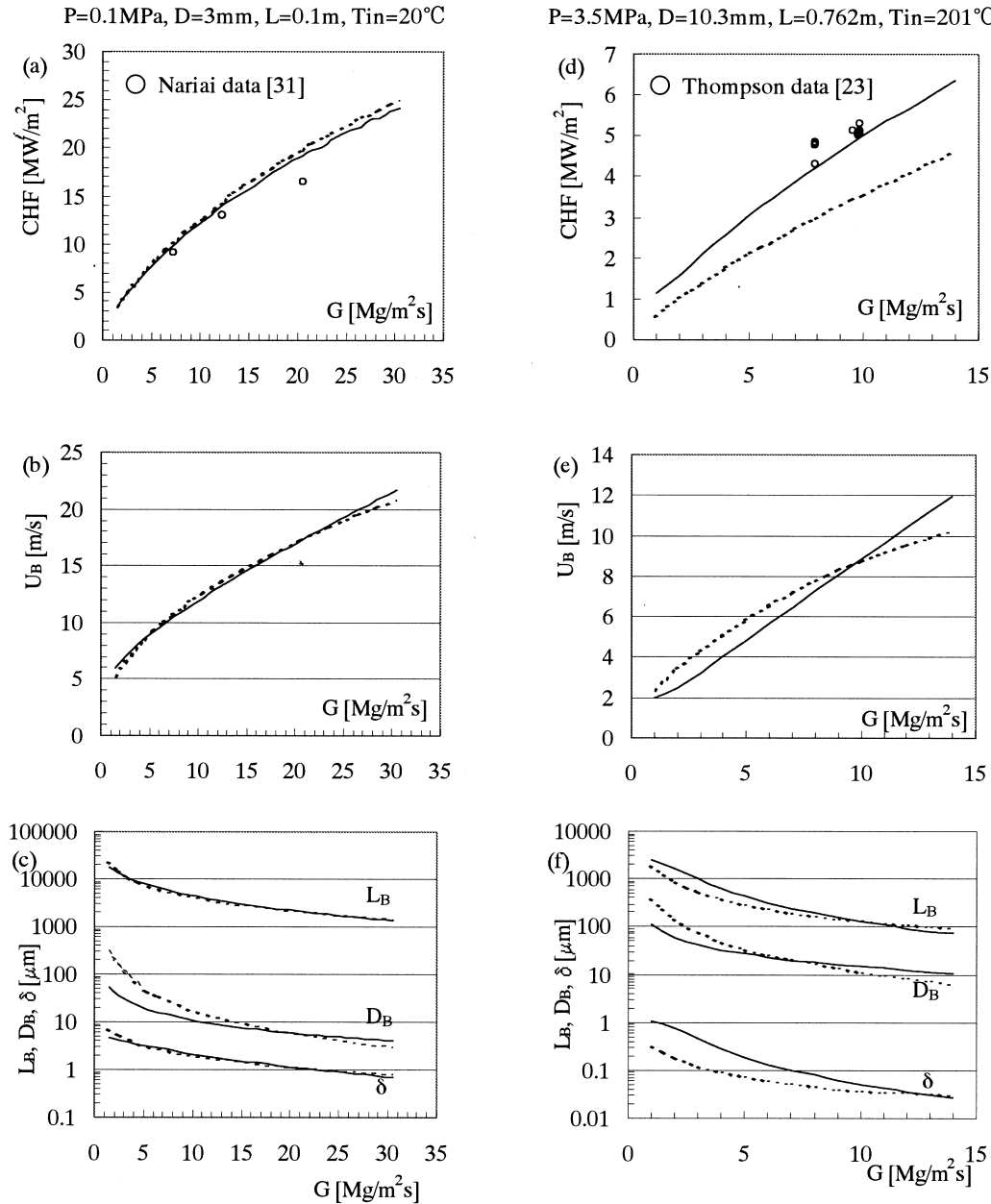


Fig. 6. Comparisons between the two models for the predictions of CHF (a, d), U_B (b, e) and L_B , D_B , δ (c, f). — The present model, - - - the Celata model.

lot. The thought that the CHF is an inverse function of inner diameter has been accepted widely. Fig. 7(d) shows the calculated CHF versus the diameter, with plotting Vandervort experimental data [29]. The model shows providing the same experimental trend of CHF versus D . From the proposed model, the trend can be explained as:

A smaller D increases subcooled liquid heat transfer coefficient, defers the NVG point and so ameliorates the exit thermal condition through:

1. Decrease the exit true quality and void fraction.
2. Decrease the exit fluid bulk temperature.

Fig. 7(d) also shows out the Celata model prediction

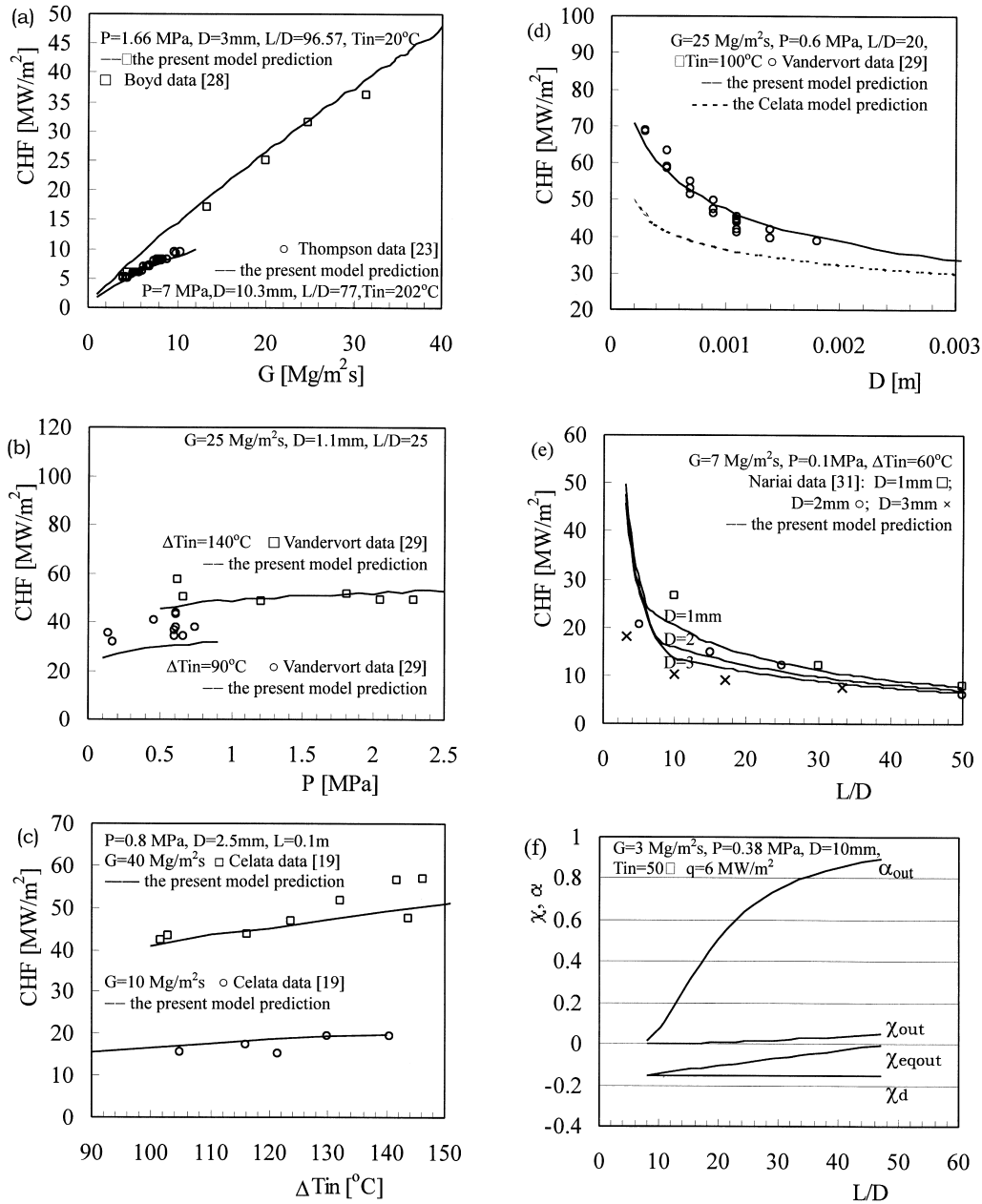


Fig. 7. Parametric trends of CHF vs.: (a) mass flux; (b) pressure; (c) inlet subcooling; (d) inner diameter; (e) ratio of heated length to diameter; (f) reason analysis for the L/D effect on the CHF.

under the same condition with a broken line. The Celata model here gives a little low CHF prediction.

5.2.2. Ratio of heated length to inner diameter L/D

From the proposed model calculation process, L/D seems giving a comprehensive and significant effect on CHF. The change of L/D will directly affect χ_{eqout} (Eq. (10a)) and ΔT_{out} (Eqs. (10e) and (10h)). The decrease of L/D will decrease χ_{eqout} and increase ΔT_{out} , ameliorate the tube exit working condition and so make the tube be able to endure a higher heat flux.

Nariai et al. [31] did an experimental research to seek the L/D effect on CHF at different inner diameter D . Fig. 7(e) shows the predicted CHF versus L/D , with comparison to the Nariai data. The present model prediction coincides the experimental data quite well. The inflection point in the prediction curve is thought as the result of substituting ΔT_{d} by ΔT_{in} when the calculated ΔT_{d} is higher than ΔT_{in} , which means the NVG occurring at the tube inlet. The phenomenon happens at almost all low L/D conditions. As a whole, the L/D effect on CHF can be concluded as:

For a certain condition, exists a threshold, beyond which the L/D do little effect on CHF and inside which the CHF increases as L/D decreases.

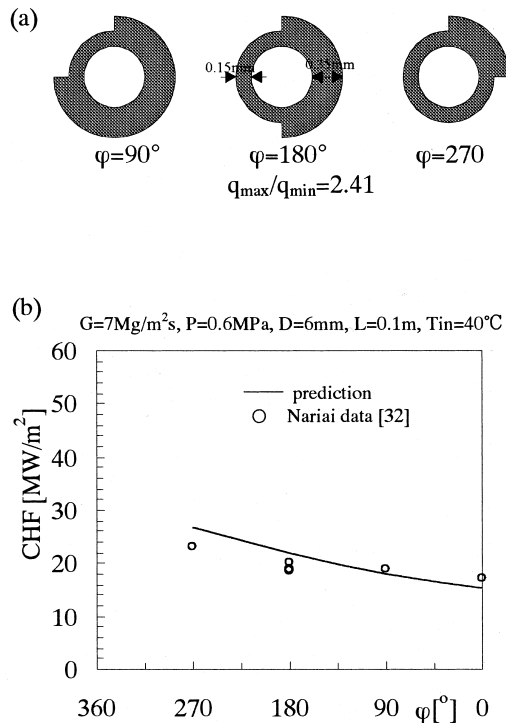


Fig. 8. (a) Peripheral non-uniform heating in Nariai experiment [32]; (b) CHF prediction for the peripheral non-uniform heating condition.

The reason for the trend is analyzed in Fig. 7(f). Except χ_{d} keeps as a constant (which is only a function of D and has no relation with L), χ_{eqout} (Eq. (10a)), χ_{out} (Eq. (10)) and α_{out} (Eq. (8)) increase with the increase of L/D . Especially, exit void fraction increases significantly. But the increasing slope slows down gradually with the increase of L/D . The L/D effect on α_{out} is considered as the main reason for the above L/D threshold effect on CHF.

Besides affecting the χ_{out} and α_{out} , L/D also affects exit liquid temperature. As shown in Eq. (10h), A increases with the increase of L/D and then the exit liquid subcooling ΔT_{out} decreases. This is considered as another reason for the above L/D effect on CHF.

6. Peripheral non-uniform heating

The effect of non-uniform heating along the circumference of the tube is of relevant importance in the thermal hydraulic design of fusion design. In Nariai et al. experiment [32], the non-uniform heating is reached by thinning a part of tube wall. Fig. 8(a) shows the cross section for the case of thinned part angle φ equals 90° , 180° , and 270° .

The peripheral non-uniform heating CHF prediction is accounted for simply in the present model by changing the heat flux q in the calculation of the NVG point with the maximum heat flux. Other calculations in which the heat flux is involved, such as in the calculation of ΔT_{out} , χ_{d} and χ_{eqout} , are made using the average heat flux. For the Nariai experiment, the average heat flux is calculated: $q_{\text{avg}} = 0.75q_{\text{max}} + 0.25q_{\text{min}}$ for $\varphi = 90^\circ$, $q_{\text{avg}} = (q_{\text{max}} + q_{\text{min}})/2$ for $\varphi = 180^\circ$ and $q_{\text{avg}} = 0.25q_{\text{max}} + 0.75q_{\text{min}}$ for $\varphi = 270^\circ$. The CHF is the maximum value of the heat flux when burnout happens.

The CHF predictions for the Nariai data are shown in Fig. 8(b). The agreement is generally good.

7. Presence of swirl flow promoters

Twist tape inserts provide a means of getting high CHF. As the presence of a twisted tape is associated with swirl flow, the liquid velocity along the flow is increased comparing with the axial velocity in straight tube. A resultant liquid velocity $V_{\gamma 1}$, was suggested by Gambill [33]. The modification is written as:

$$V_{\gamma 1} = V_1(4\gamma^2 + \pi^2)^{1/2}/(2\gamma) \quad (19)$$

where γ is the tape twist ratio.

For the twisted tape inserts give no thermal change to the tube, the increase of the velocity can be seen as the effect of the increase of the mass velocity. The pre-

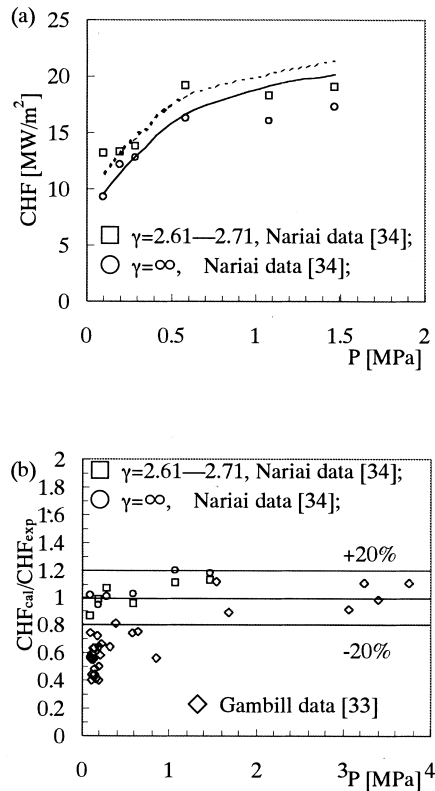


Fig. 9. CHF prediction for the twist tape inserts for (a) Nariai experiment. (b) Nariai and Gambill data.

diction is accounted by using multiple G with the same proportion as $V_{\gamma 1}$ to V_1 .

Fig. 9(a) shows the model prediction with the comparison with Nariai data [34]. The Nariai data are in the range of: $G = 6-7.5 \text{ Mg/m}^2 \text{ s}$, $D = 6 \text{ mm}$, $L = 0.1 \text{ m}$, $T_{in} = 33-45^\circ\text{C}$ and are characterized by the low mass velocity. Fig. 9(b) shows the ratio of calculated CHF to the experimental Nariai data and Gambill data [33]. The Gambill data are in the range of: $G = 15-40 \text{ Mg/m}^2 \text{ s}$, $D = 4.6-10.2 \text{ mm}$, $L = 0.063-0.4115 \text{ m}$, $T_{in} = 9-60^\circ\text{C}$ and γ from 2.08 to 4.95. The data are characterized by the high mass flux. With the Gambill modification, the proposed model seems giving good prediction to the Nariai data and the high pressure Gambill data and shows providing too low CHF prediction to low pressure-high mass flux data. The results may imply that only using the Gambill modification may not be sufficient to characterize the twist tape effect at low-pressure high mass flux condition where the swirl flow effect is significant.

As we know, tape inserts cause the swirl flow. At low mass flux, this swirl flow effect is not significant

and do not affect the near wall bubble blanket. The tape's effect can be seen as only increasing axial velocity. The proposed model is so expected to be able to predict CHF with only the modification to the mass velocity. Under such circumstance, the CHF enhancement effect should not be very significant. At high mass velocity, the swirl flow may be significant and destroys the near-wall vapor blanket. The CHF enhancement effect is, therefore, expected to be significant. For the proposed model with only the modification to the mass velocity does not reveal the true CHF mechanism under such circumstance, the model loose its rightness, giving a too low CHF prediction, as showed in Fig. 9(b).

With the increase of pressure, the vapor blanket diameter D_B and length L_B decrease. Therefore, it becomes difficult for the swirl flow to destroy the near wall vapor blanket. Under such circumstance, again, the model prediction turns possible and the CHF enhancement effect is not significant.

8. Prediction of CHF for non-water fluids

If the proposed prediction approach is soundly based, it should be capable of providing reasonable CHF predictions for fluids other than water. The proposed model is, therefore, adapted to the refrigerant 113 and liquid nitrogen system. The result is shown in the Fig. 10.

As we know, to evaluate ΔT_{lout} and χ_{out} , determining of NVG point (ΔT_d) is very important. As mentioned above, for the situation when water is used as coolant, the Ahmad model is adopted. But the Ahmad model is found unable to be used for liquid nitrogen whose enthalpy has a minus value. Therefore, for the liquid nitrogen system, the Levy model is adopted. In the R-113 CHF prediction, still the Ahmad model is adopted.

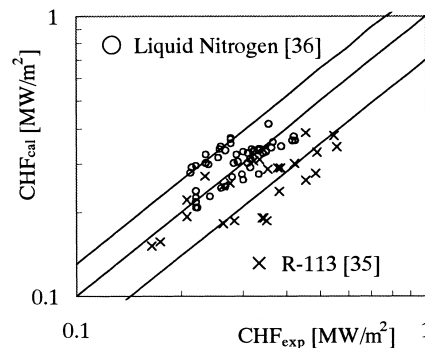


Fig. 10. CHF prediction for non-water fluids condition.

9. Discussion

1. Celata et al. [7] have raised a famous subcooled flow CHF model. They assumed the vapor blanket develops and exists only in the near-wall region where the local liquid temperature is above saturation temperature. If we take this for granted, the maximum exit void fraction should be able to be obtained from $\alpha_{\max} = \pi D y^* / (\pi D^2 / 4)$. Giving a comparison of this value with what got from the model prediction (Ahmad or Jafri model which had been tested of the general rightness). We found the former is only about 1/100 to 1/50 of the latter. Such a result made us get the thought that in subcooled flow boiling fully developed region, vapor should exist not only in the near-wall superheated area but also in the core subcooled area, and the latter one seems containing the most part of the vapor. But the success of the Celata model make us believe that, although the most part of the vapor exists in the core subcooled region, it is the less part (a

vapor blanket) that exists in the near wall region determining the CHF occurrence.

2. As we know, the accurate NVG point prediction is one of the keys for the predictions of the tube exit thermal conditions (χ_{out} , α_{out} and ΔT_{out}). It is found that in the proposed model, either the Levy or Ahmad model can be used. While with the Ahmad model, in most situations, a general better prediction is got when water is used as coolant. But this does not mean there's no problem in the use of the Ahmad model. First, as mentioned above, the Ahmad model cannot be used for the liquid nitrogen. Second, the Ahmad model shows deviation from the rightness when inlet subcooling is high enough. The analyses at $G = 4.5 \text{ Mg/m}^2 \text{ s}$, $P = 0.38 \text{ MPa}$, $D = 9.5 \text{ mm}$, $L = 0.6096 \text{ m}$, $q = 5 \text{ MW/m}^2$ condition are shown in Fig. 11(a) and (b). Although ΔT_d is substituted by ΔT_{in} when the calculated ΔT_d is higher than the ΔT_{in} (which means NVG begins at tube inlet), the Ahmad model still shows giving too high ΔT_d prediction when the inlet temperature T_{in} is low enough (Fig. 11(a)). This too high ΔT_d affects χ_d directly and results in a too low χ_d that further makes a too high abnormal χ_{out} at low inlet temperature (Fig. 11(b)). The deviation is further enlarged when α_{out} is calculated and finally results in an abnormal too high α_{out} (Fig. 11(b)). This makes the model finally gives a too low CHF prediction at low inlet temperature condition. Under above listed condition, when inlet temperature is 273.45 K (0.3°C), the prediction CHF is only 50% of experimental CHF [37]. Under such kind of low inlet temperature condition, the Levy NVG model is recommended.

From the above analysis and from the whole CHF prediction results, we here give a rough recommendation for the calculation of the NVG point.

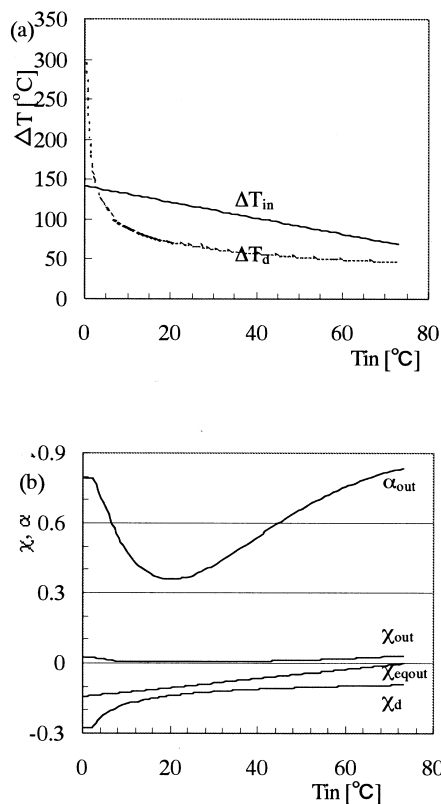


Fig. 11. The Ahmad NVG model analysis (a) too high ΔT_d value is obtained at low inlet temperature. (b) Exit thermal properties vs. inlet temperature. Abnormal increases of χ_{out} and α_{out} at low inlet temperature condition.

(a) Generally, when water is used as coolant, the Ahmad model shows a better prediction ability.

(b) The Levy NVG model is recommended at low inlet temperature ($T_{\text{in}} < 30^\circ\text{C}$).

(c) The Levy NVG model is not recommended for low mass velocity condition ($G < 2000 \text{ kg/m}^2 \text{ s}$). But the model shows better prediction ability for high mass velocity condition ($G \geq 40,000 \text{ kg/m}^2 \text{ s}$), which generally accompanied by small tube diameter).

(d) The Levy model is recommended for liquid nitrogen system.

3. Some references tend to use χ_{eqout} to substitute the inlet thermal condition (ΔT_{in} or H_{lin}) and the tube length as the subcooled flow CHF condition. But from the present model, because a certain χ_{eqout} corresponds to a series set of H_{lin} and heated length L

that only need to meet Eq. (10a), the thermal hydraulic condition can not be determined only with χ_{eqout} . A series of CHF values correspond to an χ_{eqout} condition.

So, although the heated length does not show significant effect on CHF in most situations, the heated length is a parameter independent to χ_{eqout} and should be always kept as a premise condition for subcooled flow boiling. While the χ_{eqout} and the inlet thermal parameter (ΔT_{in}), at the situation that L is known, can be substituted reciprocally.

4. It must be mentioned that under some extreme condition, such as at high pressure ($P \geq 17.5$ MPa) or high mass flux ($G \geq 50,000$ kg/m² s, with CHF up to 100 MW/m²), with the proposed model, sometimes the final calculated q does not equal to the assumed q_m even after the assumed q_m has converged to a point (this converging q_m value is the lowest possible CHF value, which is the heat flux need for the NVG point establishment at the tube exit). Although the reason for this is still not sure, a possible reason is analyzed by the present authors as: the change of the CHF triggering mechanism. The un-prediction under such circumstance may imply the CHF happens even before the NVG point, that is, happens when the bubbles still attach to the tube wall due to some other mechanism.

Actually, The CHF under such circumstance can be calculated by doing a little modification to the Levy D_B (by increasing D_B step by step, see Appendix A). Therefore, the calculated CHF is actually the heat flux for the establishment of NVG at exit. The method had been tested with Bortoli's data ([20] for high pressure condition), Ornatsuki's [40,48] data (for high G condition) and Mudawar [38] data (for extremely high G or low L/D condition). The result is astonishing good, which perhaps implies that, under such high G or high P condition, the CHF occurs before and near the NVG point.

10. Concluding remarks

A model based on the liquid sublayer dryout mechanism is proposed for the prediction of the CHF for the subcooled flow boiling. It can well predict the CHF through a wide range of physics scope. The model has been tested over a very large data bank of the CHF, showing a general good accuracy.

Unlike most references analyzing parametric trends from experiment data, the paper summarizes and interprets the trends from the model theory viewpoint. The CHF is an increasing function of the coolant subcooling and mass flux. The influence of the pressure on the

CHF turned out to be negligible. The effect of the inner diameter is to decrease the CHF as it increases. The ratio of the tube length to inner diameter L/D is ascertained to be an independent characteristic parameter on the CHF. The effect of L/D is to decrease the CHF when L/D increases, showing a threshold inside which the L/D effect is very significant while beyond which the influence of L/D is small.

Although originally developed for peripheral uniform heating and straight tube condition, the model shows good adaptation to non-uniform, twist tape insert conditions. The model also shows good CHF prediction ability for non-water system, such as liquid nitrogen and refrigerant 113 systems.

The model shows a tendency of over-prediction at low L/D condition, especially at high-pressure condition. The possible reasons are analyzed as: (1) The error in the calculations of the NVG point, exit true quality and void fraction. As we know, all the correlations for the calculation of the NVG point, true quality and void fraction are something empirical and were developed for the thermal hydraulic fully developed region. So, their suitability at low L/D condition, where thermal hydraulic is far from fully developed, is quite doubtful. (2) The change of the mechanism for the CHF occurrence. More researches for the NVG point, true quality, void fraction and CHF triggering mechanism are the keys for the accurate CHF prediction at low L/D condition.

Appendix A. CHF calculation procedure

If not specified, all properties are obtained at saturation condition.

Input $G, P, D, L, T_{\text{in}}$

Calculate friction factor f from

$$\frac{1}{\sqrt{f}} = 1.14 - 2.0 \log \left(0.75 \times 0.015 \sqrt{\frac{8\sigma\rho_f}{fG^2D}} + \frac{9.35}{Re\sqrt{f}} \right)$$

Calculate τ_w, U_τ and D_B , by:

$$\tau_w = \frac{fG^2}{8\rho_f}, \quad U_\tau = \sqrt{\frac{\tau_w}{\rho_f}}, \quad D_B = 0.015 \sqrt{\frac{\sigma D}{\tau_w}}$$

Assume a q_m :

1. Calculate NVG point

(a) Generally, calculate ΔT_d from the Ahmad model as:

$$\Delta T_d = q_m/h_{l-A}$$

where h_{l-A} is subcooled liquid-phase heat transfer coefficient in the Ahmad model and is calculated by:

$$h_{1-A} = 2.44 \frac{K_f}{D} \sqrt{\frac{GD}{\mu_f}} \left(\frac{C_{pl}\mu_f}{K_f}\right)^{1/3} \left(\frac{H_{lin}}{H_f}\right)^{1/3} \left(\frac{H_{fg}}{H_f}\right)^{1/3}$$

where H_{lin} is inlet liquid enthalpy. C_{pl} should be the specific heat at the net vapor generation point. To simplify the calculation, this C_{pl} is approximately got at inlet temperature.

(b) With the 2nd point discussed in Section 9 in the paper, if $T_{in} < 30^\circ\text{C}$ or $G \geq 40,000 \text{ kg/m}^2 \text{ s}$, calculate ΔT_d from the Levy model:

$$\Delta T_d = q_m \left(\frac{1}{h_1} - \frac{T_B^+}{C_{pf}\rho_f U_\tau} \right)$$

where

$$h_1 = 0.023 \frac{k_f}{D} \left(\frac{GD}{\mu_f}\right)^{0.8} \left(\frac{C_{pf}\mu}{k}\right)^{0.4}$$

$T_B^+ = Pr_f Y_B^+$	$0 \leq Y_B^+ \leq 5$
$T_B^+ = 5 \left\{ Pr_f + \ln \left[1 + Pr_f \left(\frac{Y_B^+}{5} - 1 \right) \right] \right\}$	$5 \leq Y_B^+ \leq 30$
$T_B^+ = 5 \left[Pr_f + \ln(1 + 5Pr_f) + 0.5 \ln \left(\frac{Y_B^+}{30} \right) \right]$	$Y_B^+ > 30$

where

$$Y_B^+ = \frac{Y_B U_\tau \rho_f}{\mu_f}, \quad Y_B = 0.015 \left(\frac{\sigma D}{\tau_w} \right)^{1/2}$$

(c) Compare ΔT_d with ΔT_{in} . If $\Delta T_d > \Delta T_{in}$, which means the physically valid net vapor generation is tube inlet, replace ΔT_d by ΔT_{in} .

(d) Calculate Z_0 (the length from the tube inlet to the net vapor generation point) by:

$$Z_0 = GDC_{pl}(\Delta T_{in} - \Delta T_d)/(4q_m)$$

C_{pl} here is specific heat at NVG.

If $Z_0 \geq L$, which means the net vapor generation point can not be reached in the tube, increase q_m and repeat the above procedures.

Significant boiling length Z_{sb} is calculated by:

$$Z_{sb} = L - Z_0$$

2. Calculate χ_{out} and α_{out}

$$A = (q_m \times Z_{sb}) / (GDC_{pl}\Delta T_d/4)$$

$$B = H_{fg} / (C_{pl}\Delta T_d)$$

The C_{pl} in the above two equations are specific heat at the NVG point.

$$\chi_{eqout} = (A - 1) / B$$

$$\chi_d = -(1/B)$$

$$\chi_{out} = \frac{\chi_{eqout} - \chi_d \exp\left(\frac{\chi_{eqout} - 1}{\chi_d}\right)}{1 - \chi_d \exp\left(\frac{\chi_{eqout} - 1}{\chi_d}\right)}$$

if $\chi_{out} \geq 1$, decrease q_m and repeat the above procedures

$$S = \left(\frac{\rho_f}{\rho_g}\right)^{0.205} \left(\frac{GD}{\mu_f}\right)^{-0.016}$$

$$\alpha_{out} = \frac{\chi_{out}}{\chi_{out} + \left(\frac{\rho_g}{\rho_f}\right) S (1 - \chi_{out})}$$

3. Calculate T_{lout}

$$T_{lout} = T_{sat} - \Delta T_d e^{(-A)}$$

if $T_{lout} \geq T_{sat}$, decrease q_m and repeat the above procedures.

4. Calculate V_c and U_B

Core region two-phase average density ρ_c , is calculated from:

$$\rho_c = (1 - \alpha_{out})\rho_{lout} + \alpha_{out} \times \rho_g$$

where ρ_{lout} is liquid density at exit temperature.

V_c is calculated as:

$$V_c = \frac{G}{\rho_c}$$

Then U_B is calculated as:

$$U_B = \frac{V_c}{1 + \sqrt{\frac{\rho_c + \rho_g}{\rho_c}}}$$

5. Calculate L_B

$$L_B = 2\pi\sigma / (\rho_g U_B^2)$$

6. Calculate U_{BL}

At low pressure ($P < 1 \text{ MPa}$):

$$U_{BL} = U_B - \sqrt{\frac{2L_B g(\rho_f - \rho_g)}{\rho_f C_D}}$$

where C_D is got by:

$$C_D = \frac{2}{3} \frac{D_B}{\left(\frac{\sigma}{g(\rho_f - \rho_g)}\right)^{0.5}}$$

Otherwise

$$U_{BL} = U_B - 2g(\rho_f - \rho_g)D_B L_B / (48\mu_f)$$

If $U_{BL} \leq 0$, increase q_m and repeat the above procedures.

7. Calculate distance y

$$\begin{cases} U_{BL}^+ = y^+ & 0 \leq y^+ < 5 \\ U_{BL}^+ = 5.0 \ln y^+ - 3.05 & 5 \leq y^+ < 30 \\ U_{BL}^+ = 2.5 \ln y^+ + 5.5 & y^+ \geq 30 \end{cases}$$

where

$$U_{BL}^+ = \frac{U_{BL}}{U_\tau}, \quad y^+ = y \frac{U_\tau}{\mu_f} \rho_f$$

8. Calculate δ

$$\delta = y - D_B/2$$

if $\delta \leq 0$, increase q_m and repeat the above procedures.

9. Calculate critical heat flux

$$q = \rho_f \delta H_{fg} U_B / L_B$$

Critical heat flux, CHF, is reached when $q_m = q$

It has been mentioned that under some extreme condition, such as at high pressure ($P \geq 17.5 \text{ MPa}$) or high mass flux ($G \geq 50,000 \text{ kg/m}^2 \text{ s}$, with CHF up to 100 MW/m^2), with the proposed model, sometimes the final calculated q doesn't equal to the assumed q_m even after the assumed q_m has converged to a point. Although the reason for this is still not sure, (Section 9, 4th point) the CHF under such circumstance can be

approximately calculated by doing a little modification to Levy D_B (by increasing D_B step by step). That is to say, if we cannot calculate CHF with the original Levy D_B , we increase D_B as $D_B = 1.01D_B$ and repeat the calculation procedure. If CHF still cannot be got, increase D_B as $D_B = 1.02D_B \dots$ until the CHF is calculated. Generally, the CHF can be got within $D_B < 1.3D_{B\text{-Levy}}$.

Appendix B. Mathematical demonstration for the equal wavelengths at the interface I and II

For a vapor blanket shown in Fig. B1.

At two gas-liquid interfaces, wave 1 and 2 exist. If c is assumed as wave velocity, λ is wave length, at any time t , wave 1 and 2 can be expressed as:

$$\eta_1 = \eta_{01} \sin k_1(x - c_1 t)$$

$$\eta_2 = D_B + \eta_{02} \sin k_2(x - c_2 t)$$

where k_1, k_2 are wave numbers and are written as:

$$k_1 = \frac{2\pi}{\lambda_1}, \quad k_2 = \frac{2\pi}{\lambda_2}$$

For η (wave height) is much smaller than wavelength λ , it can be assumed that: $k_{1,2} \eta_{1,2} = 2\pi \eta_{1,2} / \lambda_{1,2} \approx 0$

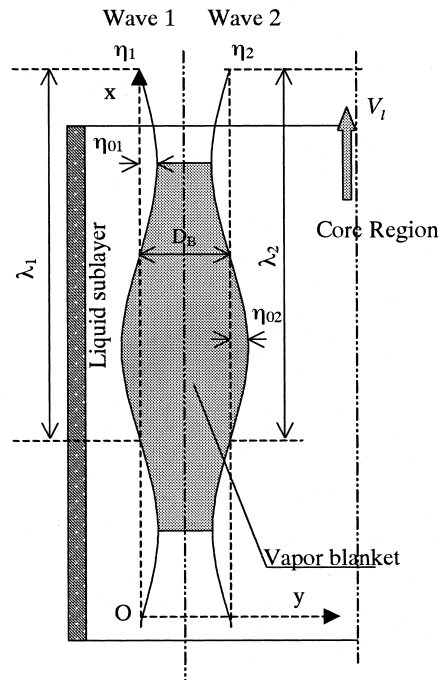


Fig. B1. Schematic representation of a vapor blanket.

To search the velocity potential ϕ of the vapor blanket, suppose the velocity on x, y directions are u and v , respectively.

$$\begin{cases} u = -\frac{\partial\phi}{\partial x} \\ v = -\frac{\partial\phi}{\partial y} \end{cases}$$

With the conservation equation:

$$\frac{\partial u}{\partial x} + \frac{\partial v}{\partial y} = -\left(\frac{\partial^2\phi}{\partial x^2} + \frac{\partial^2\phi}{\partial y^2}\right) = 0,$$

the velocity potential ϕ is written as

$$\phi = -u_B x + (A \cosh ky + B \sinh ky) \cos k(x - ct)$$

First search gas phase velocity potential from wave 1.

$$\begin{aligned} \phi_{g1} = & -u_B x + (A_1 \cosh k_1 y \\ & + B_1 \sinh k_1 y) \cos k_1(x - c_1 t) \end{aligned} \tag{B1}$$

With boundary conditions:

$$\begin{cases} y = D_B + \eta_2, v_g = -\left(\frac{\partial\phi_{g1}}{\partial y}\right)_{y=D_B+\eta_2} = \frac{d\eta_2}{dt} \\ = \frac{\partial\eta_2}{\partial t} + u_B \frac{\partial\eta_2}{\partial x}; \\ y = \eta_1, v_g = -\left(\frac{\partial\phi_{g1}}{\partial y}\right)_{y=\eta_1} = \frac{d\eta_1}{dt} = \frac{\partial\eta_1}{\partial t} + u_B \frac{\partial\eta_1}{\partial x} \end{cases}$$

A_1 and B_1 are obtained:

$$\begin{cases} A_1 = \frac{\cos k_2(x - c_2 t)}{\cos k_1(x - c_1 t)} (c_2 - u_B) k_2 \eta_{02} - (c_1 - u_B) \eta_{01} k_1 \cosh k_1 D_B \\ B_1 = (c_1 - u_B) \eta_{01} \end{cases}$$

Then search the gas phase velocity potential from wave 2:

$$\phi_{g2} = -u_B x + (A_2 \cosh k_2 y + B_2 \sinh k_2 y) \cos k_2(x - c_2 t) \tag{B2}$$

With boundary conditions:

$$\begin{cases} y = D_B + \eta_2, v_g = -\left(\frac{\partial\phi_{g2}}{\partial y}\right)_{y=D_B+\eta_2} = \frac{d\eta_2}{dt} \\ = \frac{\partial\eta_2}{\partial t} + u_B \frac{\partial\eta_2}{\partial x} \\ y = \eta_1, v_g = -\left(\frac{\partial\phi_{g2}}{\partial y}\right)_{y=\eta_1} = \frac{d\eta_1}{dt} = \frac{\partial\eta_1}{\partial t} + u_B \frac{\partial\eta_1}{\partial x} \end{cases}$$

A_2, B_2 are got as:

$$\begin{cases} A_2 = \frac{(c_2 - u_B) \eta_{02} - \frac{(c_1 - u_B) \eta_{01} k_1 \cos k_1(x - c_1 t)}{k_2 \cos k_2(x - c_2 t)} \cosh k_2 D_B}{\sinh k_2 D_B} \\ B_2 = \frac{(c_1 - u_B) \eta_{01} k_1 \cos k_1(x - c_1 t)}{k_2 \cos k_2(x - c_2 t)} \end{cases}$$

Rearranging the Eqs. (B1) and (B2) and by assuming:

$$\begin{cases} a = k_2 \eta_{02} (c_2 - u_B) \cos(k_2(x - c_2 t)) \\ b = k_1 \eta_{01} (c_1 - u_B) \cos(k_1(x - c_1 t)) \end{cases}$$

ϕ_{g1} and ϕ_{g2} are got as:

$$\begin{cases} \phi_{g1} = a \frac{\cosh k_1 y}{k_1 \sinh k_1 D_B} + b \left[\frac{\sinh k_1 y}{k_1} - \frac{\cosh k_1 y}{k_1 \tanh k_1 D_B} \right] \\ \phi_{g2} = a \frac{\cosh k_2 y}{k_2 \sinh k_2 D_B} + b \left[\frac{\sinh k_2 y}{k_2} - \frac{\cosh k_2 y}{k_2 \tanh k_2 D_B} \right] \end{cases} \tag{B3}$$

For ϕ_{g1} and ϕ_{g2} are both the gas phase velocity potential,

$$\phi_{g1} = \phi_{g2} \tag{B4}$$

The solution of Eq. (B4) is:

$$k_1 = k_2 \text{ or } k_1 = -k_2$$

For $k_1 = 2\pi/\lambda_1, k_2 = 2\pi/\lambda_2, \lambda_1 = \lambda_2$ is demonstrated.

For the two waves at the interface I and II, wave phases are determined by $k_1 c_1 t$ and $k_2 c_2 t$, respectively.

$k_1 = k_2$ means the two waves are of same phase at initial ($t = 0$) condition.

$k_1 = -k_2$ means the two waves are of opposite phase at initial ($t = 0$) condition.

In the vapor developing process, there exist a series value of time t , at which the two waves come to opposite phases.

If $k_1 = k_2$, the time t is calculated as:

$$t = \frac{(2n+1)\pi}{k|c_2 - c_1|} \quad (n = 0, 1, 2, 3 \dots)$$

If $k_1 = -k_2$, the time t is calculated as:

$$t = \frac{2n\pi}{k|c_2 - c_1|} \quad (n = 0, 1, 2, 3 \dots)$$

A stable vapor blanket is therefore assumed containing only one complete wavelength, that is to say, $L_B = \lambda$ (the length of vapor blanket equals to wavelength). Otherwise, if a vapor blanket contains more than one wavelength, the vapor blanket is assumed to be unstable. It easily breaks down to form stable vapor blanket that contains only one wavelength at the blanket thinnest points when the two waves come to the opposite phases.

References

- [1] G.P. Celata, Critical heat flux in subcooled flow boiling, in: Proceedings of 11th IHTC, vol. 1, 1998, pp. 261–277.
- [2] J. Weisman, B.S. Pei, Prediction of critical heat flux in flow boiling at low qualities, *Int. J. Heat Mass Transfer* 26 (1983) 1463–1477.
- [3] J. Weisman, S.H. Ying, Theoretically based CHF prediction at low qualities and intermediate flows, *Transaction American Nuclear Society* 45 (1983) 832–843.
- [4] J. Weisman, S. Ileslamlou, A phenomenological model for prediction of critical heat flux under highly subcooled conditions, *Fusion Technology* 13 (1988) 654–659.
- [5] C.H. Lee, I. Mudawar, A mechanism critical heat flux model for subcooled flow boiling on local bulk flow conditions, *Int. J. Multiphase Flow* 14 (1988) 711–728.
- [6] Y. Katto, A prediction model of subcooled water flow boiling CHF for pressure in the range 0.1–20.0 MPa, *Int. J. Heat Mass Transfer* 35 (1992) 1115–1123.
- [7] G.P. Celata, et al., Rationalization of existing mechanistic models for the prediction of water subcooled flow boiling critical heat flux, *Int. J. Heat Mass Transfer* 37 (Suppl. 1) (1994) 347–360.
- [8] Y. Haramura, Y. Katto, A new hydrodynamic model of critical heat flux, applicable widely to both pool and forced convection boiling on submerged bodies in saturated liquids, *Int. J. Heat Mass Transfer* 26 (1983) 389–399.
- [9] H. Kinoshita, H. Nariyai, F. Inasaka, Modeling of the subcooled flow boiling CHF in short tubes, *ICONE6-6420*, 1998.
- [10] G.P. Celata, M. Cumo, Y. Katto, A. Mariani, Prediction of the critical heat flux in water subcooled flow boiling using a new mechanistic approach, *Int. J. Heat Mass Transfer* 42 (1999) 1457–1460.
- [11] S.Y. Ahmad, Axial distribution of bulk temperature and void fraction in a heated channel with inlet subcooling, *Journal of Heat Transfer Trans. ASME* 92 (4) (1970) 595–609.
- [12] P.G. Kroeger, N. Zuber, An analysis of the effects of various parameters on the average void fractions in subcooled boiling, *Int. J. Heat Mass Transfer* 11 (1968) 211–233.
- [13] S. Levy, Forced convection subcooled boiling prediction of vapor volumetric fraction, *Int. J. Heat Mass Transfer* 10 (1967) 951–965.
- [14] P. Saha, N. Zuber, Point of net vapor generation and vapor void fraction in subcooled boiling, in: Proc. of the 5th International Heat Transfer Conference, Tokyo, 1974, p. B4.7.
- [15] F.W. Staub, et al., Heat transfer and hydraulics — the effects of subcooled voids, Final report, NYO-3679-8, 1969.
- [16] C.F. Colebrook, *J. Inst. Civil Engr* 11 (1938) 133.
- [17] T.Z. Harmathy, Velocity of large drops and bubbles in media of infinite and restricted extent, *AIChE JI* 6 (1960) 281–288.
- [18] B.K.C. Chan, R.G.H. Prince, Viscous drag on a gas bubble rise in a liquid, *AIChE JI* 11 (1965) 188–192.
- [19] G.P. Celata, et al., Assessment of correlations and models for the prediction of CHF in subcooled flow boiling, *Int. J. Heat Mass Transfer* 37 (1994) 237–255.
- [20] D. Bortoli, et al., Forced convection heat transfer burn-out studies for water in rectangular channels and round tubes at pressures above 500 psia, WAPD-188, 1958.
- [21] B. Matzner, Basic experimental studies of boiling fluid flow and heat transfer at elevated pressure, T.I.D. 18978, 1963.
- [22] D.H. Lee, J.D. Obterelli, An experimental investigation of forced convection burnout in high pressure water, Part 1, Round tube with uniform flux distribution, AEEW-R213, 1963.
- [23] R.V. Thompson, Boiling water heat transfer burnout in uniformly heat round tubes: a compilation of world data with accurate correlations, AEEW-R356, 1964.
- [24] R.J. Weatherhead, Heat transfer flow instability and critical heat flux in a small tube at 200 psia, A.N.L. 6715, 1963.
- [25] R.J. Weatherhead, Nucleate boiling characteristics and critical heat flux occurrence in sub-cooled axial-flow water systems, A.N.L. 6675, 1963.
- [26] R.R. Hood, L. Isakoff, Heavy water moderate power reactors progress report for June 1962, D.P. 755.
- [27] Y.Z. Chen, R.B. Zhou, L.M. Hao, H.Y. Chen, Critical heat flux with subcooled boiling of water at low pressure, in: Eighth International Topical Meeting on Nuclear Reactor Thermal-Hydraulics, vol. 2, 1997, pp. 958–964.
- [28] R.D. Boyd, Subcooled water flow boiling at 1.66 MPa under uniform high flux conditions, in: Proc. of the ASME Winter Annual Meeting, HTD, vol. 119, 1989, pp. 9–15.
- [29] C.L. Vandervort, A.E. Bergles, M.K. Jensen, The ulti-

- mate limits of forced convective subcooled boiling heat transfer, RPI Interim Report HTL-9 DE-FG02-89ER 14019, 1992.
- [30] B.S. Pei, Prediction of critical heat flux in flow boiling at low qualities, dissertation submitted to the Department of Chemical and Nuclear Engineering, College of Engineering, Division of Graduate Education and Research, University of Cincinnati, 1981.
- [31] H. Nariai, F. Inasaka, T. Shimura, Critical heat flux of subcooled flow boiling in narrow tube, in: Proc. of the 1987 ASME-JSME Thermal Engineering Joint Conference, 1987, pp. 455–462.
- [32] H. Nariai, F. Inasaka, A. Ishikawa, H. Kinoshita, Effect of internal twisted tape on critical heat flux of subcooled flow boiling under non-uniform heating condition, Trans. JSME (B) 60 (1994) 4215–4221 (in Japanese).
- [33] W.R. Gambill, R.D. Bundy, R.W. Wansbrough, Heat transfer, burnout and pressure drop for water for swirl flow through tubes with internal twisted tapes, Chem. Eng. Progress Symposium Series 57 (1961) 127–137.
- [34] H. Nariai, F. Inasaka, W. Fujisaki, H. Ishiguro, Critical heat flux of subcooled flow boiling in tubes with internal twisted tapes, in: 7th Proc. of Nuclear Thermal Hydraulics, 1991, pp. 38–46.
- [35] R.D. Coffield Jr, W.M. Rohrer Jr, L.S. Tong, A subcooled DNB investigation of freon-113 and its similarity to subcooled water DNB data, Nuclear Engineering and Design 11 (1969) 143–153.
- [36] S. Stephen, J. Robert, D. Dweght, Buoyancy effects on critical heat flux of forced convective boiling in vertical flow, NASA TN D-3672, Washington DC, Oct. 1966.
- [37] D.H. Knobel, S.D. Harris, B. Crain, Jr., R.M. Biderman, Forced-convection subcooled critical heat flux, DP-1306, E.I. Dupont de Nemours and Company, Feb. 1973.
- [38] I. Mudawar, M.B. Bowers, Ultra-high critical heat flux (CHF) for subcooled water flow boiling — I: CHF data and parametric effects for small diameter tubes, Int. J. Heat Mass Transfer 42 (1999) 1405–1428.
- [39] T. Jafri, T.J. Dougherty, B.W. Yang, Correlation of critical heat flux data for uniform tubes, in: Proceedings of the 7th International Meeting on Nuclear Reactor Thermal-Hydraulics, Sept. 1995, NURETH-7, NUREG/CP-0142, vol. 4, 1995, pp. 3197–3217.
- [40] A.P. Ornatskii, L.S. Vinyarskii, Heat transfer crisis in forced flow under heated water in small-bore tubes, High Temperature 3 (3) (1965) 444–451.
- [41] F. Inasaka, H. Nariai, Critical heat flux of subcooled flow boiling with water, Proc. of the NURETH-4 1 (1989) 115–120.
- [42] R.D. Boyd, Subcooled water flow boiling experiments under uniform high flux conditions, Fusion Technology 13 (1988) 121–142.
- [43] R.D. Boyd, Subcooled water flow boiling transition and the L/D effect on CHF for a horizontal uniformly heated tube, Fusion Technology 18 (1990) 317–324.
- [44] A. Achilli, G. Cattadori, G.P. Gaspari, Subcooled burnout in uniformly and non-uniformly heated tubes, in: European Two-phase Flow Group Meeting, Paper C2, Stockholm, June, 1992, pp. 1–3.
- [45] W.R. Gambill, N.D. Greene, Boiling burnout with water in vortex flow, Chemical Engineering Progress 54 (10) (1958) 68–76.
- [46] C.S. Loosemore, B.C. Skinner, Subcooled critical heat flux for water in round tube, S.M. Thesis, Massachusetts Institute of Technology, Cambridge, MA, 1965.
- [47] A.P. Ornatskii, A.M. Kichigan, Critical thermal loads during the boiling of subcooled water in small diameter tubes, Teploenergetika 6 (1962) 75–79.
- [48] A.P. Ornatskii, The influence of length and tube diameter on critical heat flux for water with forced convection and subcooling, Teploenergetika 4 (1960) 67–69.
- [49] S. Mishak, W.S. Durant, R.H. Towell, Heat flux at burnout, DP-35, E.I. Dupont de Nemours and Company, 1959.
- [50] D.F. Babcock, Heavy water moderated power reactors, DP-725, E.I. Dupont de Nemours and Company, 1962.
- [51] E. Burck, W. Hufschmidt, EUR-2432 d, Euratom, 1965.
- [52] J. Mayersak, S.D. Raezer, E.A. Bunt, Confirmation of Gambill–Greene straight flow burnout heat flux equation at high flow velocity, Trans. ASME J. Heat Transfer 86 (1964) 420–425.
- [53] J.W. Schaefer, J.R. Jack, Investigation of forced-convection nuclear boiling of water for nozzle cooling at very high flux, Technical Note D-1214, NASA, 1962.
- [54] E.J. Thorgerson, Hydrodynamic aspect of the critical heat flux in subcooled convection boiling, PhD thesis, University of South Carolina, 1969.
- [55] Y.A. Zeigarnik, N.P. Privalov, A.L. Klimov, Critical heat flux with boiling of subcooled water in rectangular-channel with one-sided supply of heat, Thermal Engineering 28 (1) (1981) 40–42.
- [56] G.E. Dix, Vapor void fractions for forced convection with subcooled boiling at low flow rates, NEDO-10491, General Electric Company, 1971.